

# 介质微球光场调控制备多级银微纳结构及其表面增强拉曼光谱研究(特邀)

陈冰冰, 闫胤洲\*, 赵晨, 赵艳, 蒋毅坚

北京工业大学材料与制造学部激光工程研究院, 北京 100124

**摘要** 表面增强拉曼光谱(SERS)是一种高灵敏的分子振动指纹光谱技术。光辅助化学还原制备SERS衬底具有成本低、环境适用性强等优势,但在微纳结构多样化制造方面存在局限性,限制了SERS衬底的检出性能。笔者系统研究了介质微球独特的聚焦特性,揭示了微球直径对聚焦光场分布的调控规律,在微球底部实现了可控的光场空间分布,实现了多级银微纳结构的快速光还原合成。进一步,通过优化制备参数(前驱液浓度比、激光辐照功率及辐照时间),成功制备了具有优异拉曼增强效果的多级银纳米颗粒/银微环/介质微球(AgNPs/AgMRs/MS)复合结构。通过介质微球和多级银微纳结构(AgNPs/AgMRs)中的光场耦合,即微球聚焦、多级银微纳结构局域表面等离子体共振以及复合结构定向发射等,实现了 $10^{-14}$  mol/L的痕量检测,增强因子可达 $9.50 \times 10^9$ ,为光化学还原制备高性能介质-金属复合SERS衬底提供了新思路。

**关键词** 光谱学; 表面增强拉曼光谱; 多级银微纳结构; 光化学还原; 介质微球

中图分类号 O59 文献标志码 A

DOI: 10.3788/CJL231382

## 1 引言

表面增强拉曼光谱(SERS)作为一种光学无损分析技术,以灵敏度高与特异性强的特点被广泛应用于环境检测、食品安全、医学诊断、文化遗产保护等领域<sup>[1-4]</sup>。常见的SERS衬底利用金属纳米结构与光场耦合形成局域表面等离子体共振(LSPR),实现分子拉曼信号的显著增强<sup>[5-6]</sup>。通过设计和制备不同形貌的金属纳米结构可以实现LSPR效应的可控调节,进而调控SERS的增强能力。

目前,SERS衬底包括“自上而下”和“自下而上”两种制造方式<sup>[7]</sup>。“自上而下”制造方法主要包括飞秒激光表面微纳结构制造<sup>[8]</sup>、脉冲激光烧蚀<sup>[9]</sup>、电子束刻蚀<sup>[10]</sup>等,所制备的SERS衬底可以实现低至 $10^{-17}$  mol/L的单分子检测,但较为复杂的制造流程导致SERS衬底成本增加。“自下而上”的制造方式通常是通过环境控制纳米颗粒的形核生长,主要包括化学还原法<sup>[11]</sup>、光化学还原法<sup>[12]</sup>、电化学还原法<sup>[13]</sup>、溶胶-凝胶法<sup>[14]</sup>等,具有产量大、制造成本低等优势。其中,光还原金属离子制备纳米结构技术因具有产物化学成分纯净、工艺可控性高<sup>[15]</sup>的特点而备受关注。然而,该技术采用非相干光源(例如LED或氙弧灯)还原金属纳米结构,不仅

效率不高<sup>[16-17]</sup>,而且结构可控性依赖于化学自组装过程,从而导致该技术在SERS衬底结构多样性设计以及实际应用方面存在诸多限制。激光光源具有相干性好、功率高、方向性好等特点,在光化学还原法中被广泛使用,已有研究人员采用以激光作为光源的光化学还原法在多种材料表面实现了金属纳米结构SERS衬底的制备。

激光化学还原法通过调控前驱液浓度、激光波长、辐照功率以及辐照时间等参数在聚合物薄膜<sup>[18-19]</sup>、玻璃<sup>[20]</sup>等介质中原位还原金属离子,但该过程通常需要高功率连续激光实现快速原位还原。利用金属等离子体激发的近场电磁增强效应<sup>[21]</sup>、载流子激发效应<sup>[22]</sup>、缺陷诱导效应<sup>[23]</sup>等可以有效降低还原过程所需的激光功率需求<sup>[24]</sup>。随着大功率飞秒脉冲激光技术的发展,基于双光子吸收的飞秒激光直写技术在图案化金属纳米结构还原合成领域得到了广泛关注<sup>[25-29]</sup>,其最大优势是能够在封闭的微通道中一步制备SERS衬底,而且所制备的SERS衬底可以达到 $10^{-13}$  mol/L的拉曼检测能力;但该方法存在聚焦加工区域小、效率较低的问题,不适合用于金属微纳结构的大面积制造<sup>[30]</sup>。空间光整形技术可在一定程度上提高图案化微加工效率<sup>[28,31]</sup>,但仍难以平衡合成效率、图案精度以及制造尺

收稿日期: 2023-11-09; 修回日期: 2023-12-15; 录用日期: 2023-12-25; 网络首发日期: 2024-01-13

基金项目: 国家重点研发计划(2022YFB4600400)、国家自然科学基金(12074019)、北京市教委科技计划重点项目(KZ202110005002)

通信作者: \*yyan@bjut.edu.cn

度之间的内在固有矛盾。因此,一步法激光快速还原图案化微纳结构成为目前亟待突破的技术瓶颈。

以介质微球为代表的光学微腔具有丰富的光场调控特性,可以对入射光场进行高效并行调控,产生光子纳米射流(PNJ)<sup>[32]</sup>、光学回音壁共振模式(WGM)<sup>[33]</sup>和光学定向天线(DA)<sup>[34]</sup>等一系列独特的光学效应。介质微球产生的光子纳米射流效应可在微球底部实现近场光场聚焦,产生超越衍射极限的光场分布<sup>[35]</sup>。曼切斯特大学的李琳、新加坡国立大学的洪明辉等团队展示了介质微球阵列的激光并行微纳制造能力<sup>[35-36]</sup>。介质微球独特的光场调控特性在SERS衬底制备方面同样得到了广泛关注。2007年,陆永枫团队<sup>[37]</sup>利用介质微球阵列的光子纳米射流效应实现了拉曼增强。本课题组前期从理论和实验上揭示了介质微球的光学回音壁以及定向天线效应对拉曼增强的贡献<sup>[38-39]</sup>。然而,仅采用介质微球光场调控所获得的拉曼增强效果远不及金属纳米结构的LSPR效应。因此,将金属纳米结构与介质微球耦合形成介质-金属复合SERS衬底,是实现高灵敏度拉曼检测的重要技术路线。目前,将金属纳米结构与介质微球耦合的方法大多是将金属纳米颗粒通过物理溅射或自组装的方式沉积到微球表面<sup>[40-41]</sup>,但所得到的金属纳米结构较为单一,LSPR的拉曼增强能力不能充分展现。因此,在介质微球表面构建具有丰富“热点”的多级金属微纳结构,是突破高

性能介质-金属复合SERS衬底制造瓶颈的有效方案。

笔者提出了一种银纳米颗粒(AgNPs)/银微环(AgMRs)/钛酸钡微球(MS)多级介质-金属复合SERS衬底的激光快速还原合成方法。通过介质微球聚焦入射激光,在微球底部实现对入射光场的跨尺度调控并诱导还原多级银微纳结构(AgNPs/AgMRs),最终获得了具有优异拉曼增强效果的多级AgNPs/AgMRs/MS复合结构。本研究为快速制备高性能复合SERS衬底提供了新思路。

## 2 实验方法

### 2.1 样品制备

本工作的基本制造思路为:通过介质微球聚焦入射激光,在微球底部形成具有特定空间分布的光场,进而诱导光还原实现多级银微纳结构的可控合成。具体制备步骤如图1所示:

1) 将聚二甲基硅氧烷(PDMS)与固化剂按质量比10:1混合并搅拌均匀,在真空干燥箱中静置(去除气泡);接着将PDMS胶体溶液滴在清洁的盖玻片上,以1000 r/m的速度旋涂20 s,在加热平台上以100 °C固化20 min,形成厚度约为150 μm的PDMS薄膜衬底;之后采用机械研磨自组合法将钛酸钡微球(MS,直径为5~22 μm,购自Cosphereic)均匀地铺于PDMS

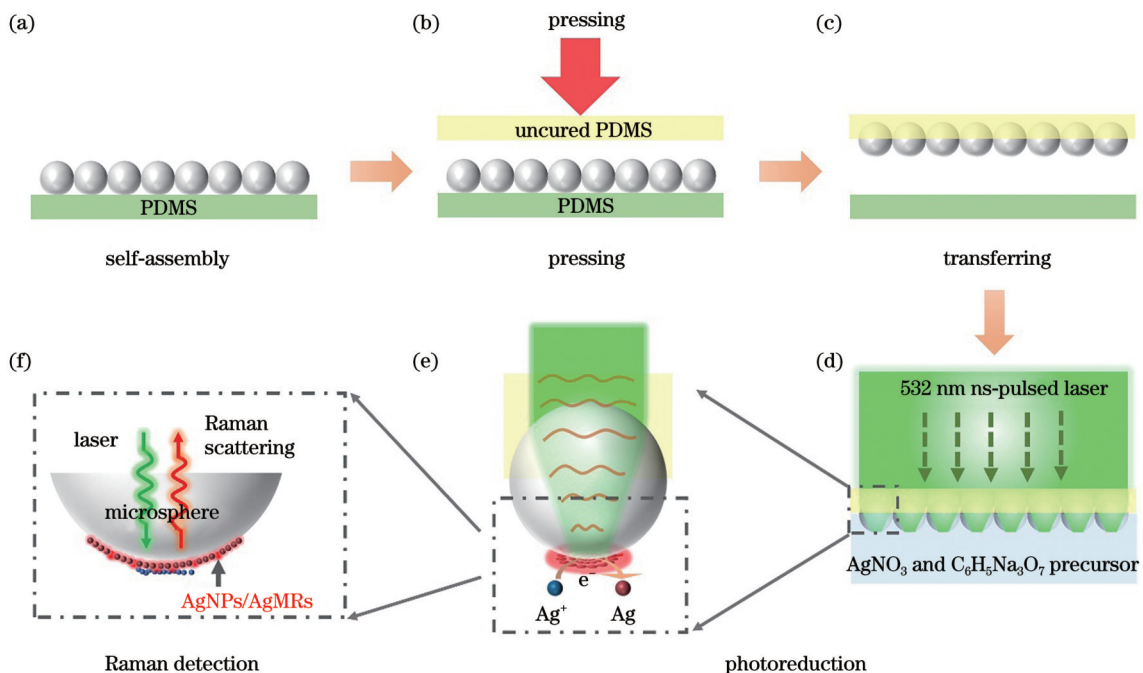


图1 介质微球聚焦激光诱导还原多级银微纳结构示意图。(a)介质微球自组装于PDMS薄膜表面;(b)~(c)介质微球嵌入并转移至未固化PDMS薄膜中;(d)~(e)激光还原合成银纳米颗粒(AgNPs)/银微环(AgMRs)/钛酸钡微球(MS)复合SERS衬底;(f)拉曼检测

Fig. 1 Schematics of laser-induced chemical reduction for hierarchical silver micro-nanostructures by dielectric microsphere focusing. (a) Self-assembly of dielectric microspheres on the surface of PDMS film; (b)–(c) dielectric microspheres were embedded into the uncured PDMS film; (d)–(e) preparation of AgNPs/AgMRs/MS SERS substrates by laser-chemical reduction; (f) Raman detection

薄膜表面上,形成单层密铺阵列结构,如图 1(a)所示。

2) 将 PDMS 胶体溶液滴在清洁的盖玻片上,以 1300 r/m 的速度高速旋涂 20 s,接着在加热平台上以 100 °C 固化 1 min,得到未固化的 PDMS 薄膜。

3) 将未固化的 PDMS 薄膜倒置于高折射率钛酸钡微球阵列表面,施加压力,将微球阵列转移并半嵌入未固化的 PDMS 薄膜中(PDMS/MS),并将 PDMS/MS 在 100 °C 下加热 20 min 使之完全固化,如图 1(b)~(c)所示。

4) 将硝酸银溶液( $\text{AgNO}_3$ , 购自赛默飞世尔(中国)科技有限公司)与柠檬酸三钠( $\text{C}_6\text{H}_5\text{Na}_3\text{O}_7$ , 购自 Alfa Aesar)用去离子水混合均匀,得到银前驱液;然后将 532 nm 连续激光经 PDMS/MS 聚焦于银前驱液中,激光功率控制在 49~168  $\mu\text{W}$ ,如图 1(d)所示。

5) 在激光还原反应作用下,银离子在微球底部聚焦光场分布区域诱导还原多级银微纳结构,获得介质-金属复合 SERS 衬底,如图 1(e)所示。

6) 用超纯水清洗介质-金属复合 SERS 衬底 2 min 后,对待检分子溶液进行拉曼检测,如图 1(f)所示。

## 2.2 样品表征

采用扫描电子显微镜(GeminiSEM 300)表征多级银微纳结构的表面形貌。采用中国科学院半导体研究所研制的 SmartRaman 共焦显微拉曼系统采集拉曼光谱,采用 10 $\times$ 物镜(Olympus MPlan N, 数值孔径  $NA=0.25$ )以背散射模式采集拉曼信号,并在配备有 600 line/mm 光栅的高分辨光谱仪(Horiba LabRAM iHR550)上进行信号分析。激发光源采用 633 nm 窄线宽 He-Ne 连续激光器(Thorlabs, HNL100L He-Ne 激光器),激光经显微系统到达样品表面的功率固定为 168  $\mu\text{W}$ ,聚焦光斑直径为 10.49  $\mu\text{m}$ ,光谱采集时间固定为 10 s,采集光谱范围为 400~1800  $\text{cm}^{-1}$ 。

## 2.3 数值模拟

利用 COMSOL Multiphysics 进行电磁场数值模拟,在射频模块中建立与 PDMS/MS 和 AgMRs/MS 几何形状相同的二维截面模型,利用 532 nm 及 633 nm 平面波和电偶极子激励分别对激发光源和散射光源进行模拟,采用周期性边界条件模拟微球阵列结构。模

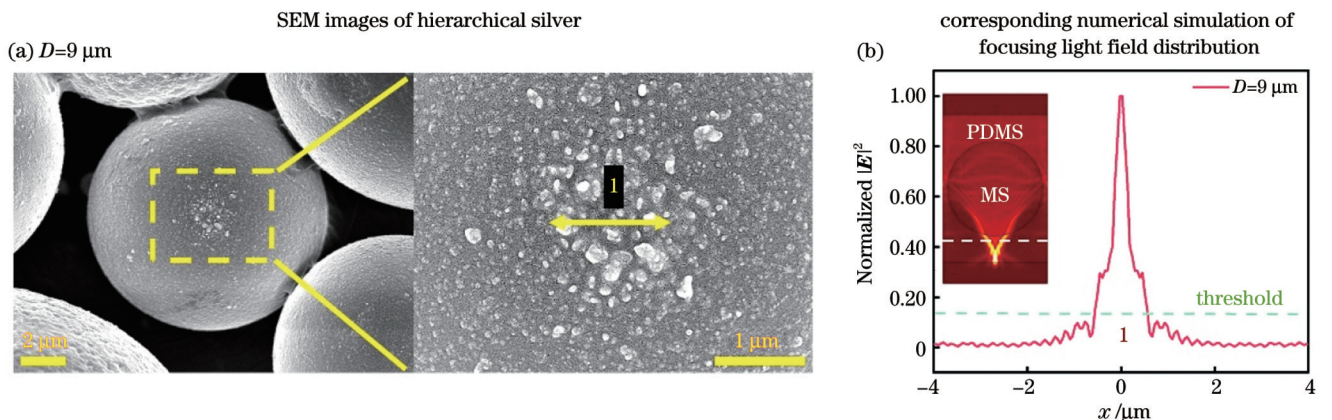
型中介质微球的直径为 9~52  $\mu\text{m}$ ,钛酸钡微球、PDMS 薄膜、 $\text{H}_2\text{O}$ 、空气的折射率分别为 1.9、1.4、1.33、1,其中银在 532 nm 和 633 nm 波长处的折射率分别为  $0.14+3.06i$  和  $0.15+4.02i$ <sup>[42]</sup>。采用有限元数值模拟获得各类结构中光场的空间分布和远场发射结果。

## 3 分析与讨论

利用介质微球的聚焦特性在微球底部形成具有特定空间形貌的光场分布,通过实验和数值模拟揭示微球直径对空间光场分布的调控以及激光化学还原参数对银微纳结构成形的作用规律,在微球底部实现与光场分布一致的多级银微纳结构的一步法可控合成,获得 AgNPs/AgMRs/MS 复合结构。之后,对 AgNPs/AgMRs/MS 复合结构的拉曼增强能力进行表征与优化,揭示其拉曼增强机制。基于该 AgNPs/AgMRs/MS 复合结构,最终获得了高性能的介质-金属复合 SERS 衬底。

### 3.1 介质微球直径对银微环(AgMRs)结构的调控

介质微球聚焦效果受微球直径的影响<sup>[43]</sup>。通过改变微球直径在微球底部实现聚焦光斑光场的调控,从而获得不同的 AgMRs 结构。图 2(a)、(c)、(e)、(g)、(i)、(k)展示了在  $\text{AgNO}_3$  与  $\text{C}_6\text{H}_5\text{Na}_3\text{O}_7$  浓度比( $C_{\text{AgNO}_3}:C_{\text{C}_6\text{H}_5\text{Na}_3\text{O}_7}$ )为 1:4、激光辐照功率为 98  $\mu\text{W}$ 、辐照时间为 80 s 的条件下,介质微球底部还原的 AgMRs 的表面形貌随微球直径的变化规律。可以发现:当微球直径( $D$ )为 9  $\mu\text{m}$  时,只形成了 AgNPs,无 AgMRs 形成;当微球直径增大至 14  $\mu\text{m}$  时,形成了单 AgMRs 结构;继续增大微球直径至 17  $\mu\text{m}$  时,形成了双层嵌套 AgMRs;当微球直径为 21  $\mu\text{m}$  时,微球底部形成了直径约为 4.5  $\mu\text{m}$  的三层嵌套 AgMRs 结构。图 2(b)、(d)、(f)、(h)为不同直径介质微球聚焦光场分布的数值模拟结果。表 1 展示了不同微球直径下实验与模拟得到的 AgMRs 宽度(数字 1~3)和 AgMRs 间隙(数字 4~6)的特征尺寸,结果表明:介质微球底部聚焦光场还原能量阈值截线处形成的环结构与实验获得的 AgMRs 尺寸一致。但当介质微球直径进一步增大到 39  $\mu\text{m}$  和 52  $\mu\text{m}$  时,由于焦点远离微球底部,较弱的光



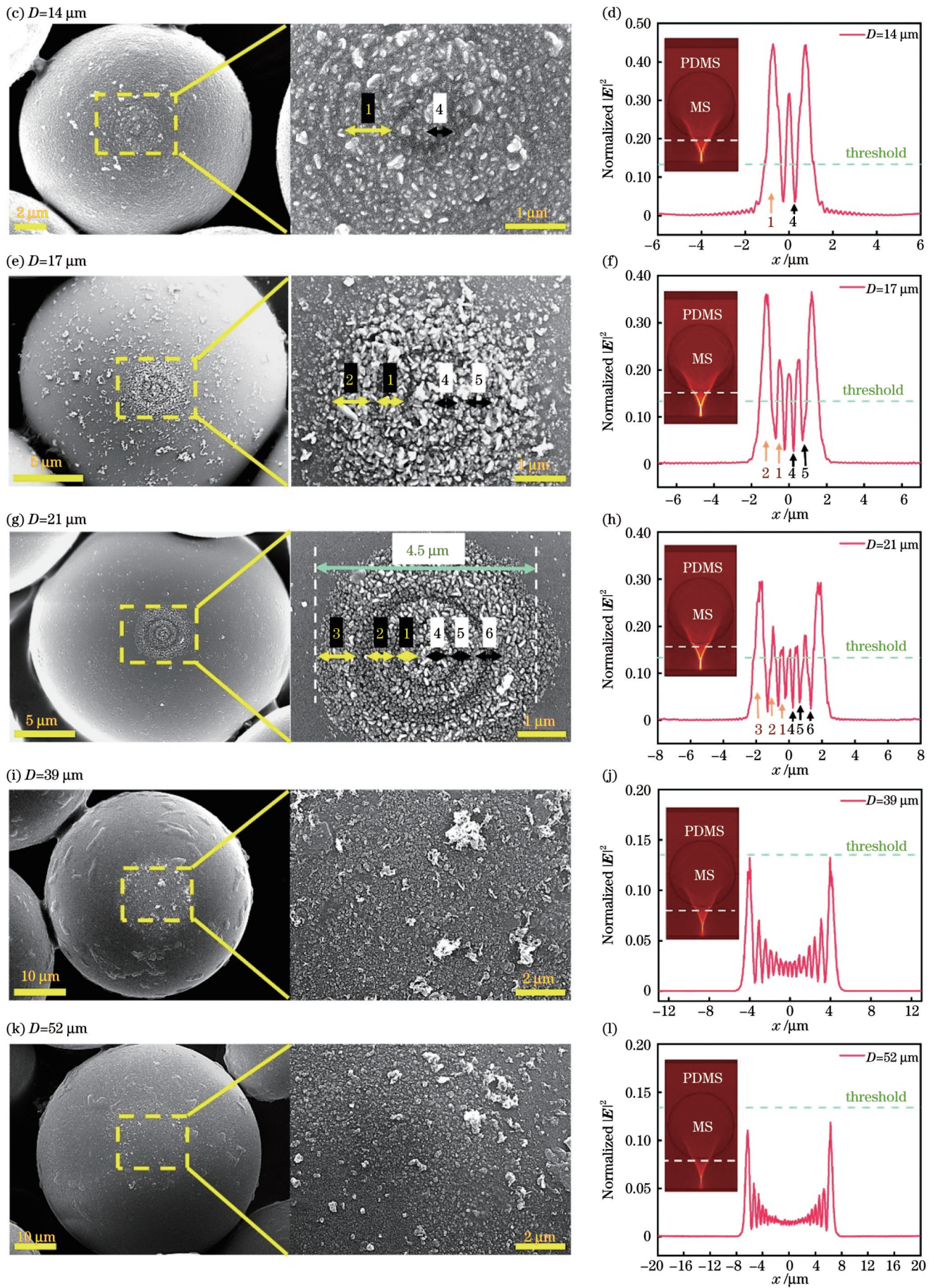


图 2 介质微球直径( $D$ )对 AgNPs/AgMRs 特征结构的调控规律  
 Fig. 2 Regulation of dielectric microsphere diameter ( $D$ ) on the structure of AgNPs/AgMRs

表 1 实验和模拟得到的不同直径介质微球底部 AgMRs 的特征尺寸分布

Table 1 Experimental and simulated characteristic size of AgMRs under dielectric microspheres with different diameters

| Data source | Region | Characteristic size / nm |                     |                     |                     |
|-------------|--------|--------------------------|---------------------|---------------------|---------------------|
|             |        | $D=9\ \mu\text{m}$       | $D=14\ \mu\text{m}$ | $D=17\ \mu\text{m}$ | $D=21\ \mu\text{m}$ |
| Experiment  | 1      | 1209±61                  | 790.5±80.9          | 334.5±32.5          | 267.1±23.4          |
|             | 2      |                          |                     | 685.2±36.1          | 423.9±28.9          |
|             | 3      |                          |                     |                     | 862.4±51.3          |
|             | 4      |                          | 87.0±10.0           | 97.0±11.7           | 70.6±15.7           |
|             | 5      |                          |                     | 133.5±15.9          | 98.2±13.3           |
|             | 6      |                          |                     |                     | 121.4±20.1          |
| Simulation  | 1      | 1126                     | 519.8               | 328.9               | 342.1               |
|             | 2      |                          |                     | 712.8               | 479.3               |
|             | 3      |                          |                     |                     | 890.2               |
|             | 4      |                          | 82.2                | 79.9                | 94.9                |
|             | 5      |                          |                     | 126.1               | 90.5                |
|             | 6      |                          |                     |                     | 134.7               |

场能量无法达到光还原阈值能量,微球表面还原的 AgNPs 显著减少,无法形成 AgMRs 结构,如图 2(i)~(l)所示。这一结果证明介质微球通过聚焦入射激光在微球底部实现了对入射光场的微米尺度调控并诱导还原了 AgMRs。当微球直径为 21  $\mu\text{m}$  时,可以得到多至三层嵌套的 AgMRs,AgMRs 内部由 AgNPs 组成,AgNPs/AgMRs 中的银间隙可能会产生大量 SERS “热点”区域。

### 3.2 光化学还原参数对多级 AgNPs/AgMRs/MS 复合结构表面形貌的影响

为得到光化学还原工艺参数(前驱液浓度比  $C_{\text{AgNO}_3}:C_{\text{C}_6\text{H}_5\text{Na}_3\text{O}_7}$ 、激光辐照功率、辐照时间)对多级银微纳结构的影响,固定激光辐照功率为 98  $\mu\text{W}$ ,在不同辐照时间下,研究了  $C_{\text{AgNO}_3}:C_{\text{C}_6\text{H}_5\text{Na}_3\text{O}_7}$  对多级银微纳结构形貌的调控规律。分析图 3(a)可以发现:当  $C_{\text{AgNO}_3}:C_{\text{C}_6\text{H}_5\text{Na}_3\text{O}_7}=1:2$  时,AgNPs 生长缓慢;当  $C_{\text{AgNO}_3}:C_{\text{C}_6\text{H}_5\text{Na}_3\text{O}_7}=1:6$  时,密集的 AgNPs 可以在 40 s 内迅速形成,导致 AgMRs 结构不清晰;当  $C_{\text{AgNO}_3}:C_{\text{C}_6\text{H}_5\text{Na}_3\text{O}_7}=1:4$  时,AgNPs 生长速度适中,生成的 AgMRs 结构清晰。因此,在  $C_{\text{AgNO}_3}:C_{\text{C}_6\text{H}_5\text{Na}_3\text{O}_7}=1:4$  的基础上,探究了激光辐照功率和辐照时间对多级银微纳结构的影响。图 3(b)表明:当辐照功率较小(49  $\mu\text{W}$ )时,还原出的 AgNPs 数量少,无法形成 AgMRs 结构。当辐照功率为 98  $\mu\text{W}$  时,AgNPs 的还原速度明显提高,辐照 40 s 时形成了以 50 nm 直径为主的 AgNPs;当辐照时间延长至 80 s 时,可观察到清晰的 AgMRs 结构,同时 AgNPs 的密集程度明显增加,产生了大量细小的纳米间隙;进一步将辐照时间延长到 120 s,可以发现 AgNPs 尺寸明显变大。当激光功率为 168  $\mu\text{W}$  时,辐照 40 s 即可观察到清晰的多级银微纳结构;随着辐照时间延长,AgMRs 结构逐渐被 AgNPs 填充,当辐照时间延长至 120 s 时,

AgNPs 过度生长,导致 AgMRs 结构消失。通过对光化学还原工艺参数进行优化得出:在  $C_{\text{AgNO}_3}:C_{\text{C}_6\text{H}_5\text{Na}_3\text{O}_7}=1:4$ 、激光辐照功率为 98  $\mu\text{W}$ 、辐照时间为 80 s 的条件下,可以获得具有清晰 AgMRs 结构及高密度 AgNPs 的多级银微纳结构。

### 3.3 多级 AgNPs/AgMRs/MS 复合结构的 SERS 性能优化

以浓度为  $10^{-6}$  mol/L 的亚甲基蓝(MB)溶液为待检测物,研究了不同制备工艺下多级 AgNPs/AgMRs/MS 复合结构的拉曼性能。图 4(a)展示了不同  $C_{\text{AgNO}_3}:C_{\text{C}_6\text{H}_5\text{Na}_3\text{O}_7}$  下 1624  $\text{cm}^{-1}$  拉曼峰强度的变化曲线,可以发现当  $C_{\text{AgNO}_3}:C_{\text{C}_6\text{H}_5\text{Na}_3\text{O}_7}$  为 1:4~1:6 时具有最优的拉曼增强效果。在  $C_{\text{AgNO}_3}:C_{\text{C}_6\text{H}_5\text{Na}_3\text{O}_7}=1:4$  下,进一步研究了光化学还原激光辐照功率对拉曼增强性能的影响,如图 4(b)所示。结果表明:与 49  $\mu\text{W}$  和 168  $\mu\text{W}$  相比,在 98  $\mu\text{W}$  辐照功率下得到的多级 AgNPs/AgMRs/MS 复合结构的拉曼增强性能更好;拉曼强度随辐照时间延长呈先增大后下降的现象,在辐照 80 s 时可获得最佳的拉曼增强性能。这一辐照时间与获得最优多级银微纳结构的辐照时间一致。之后,通过改变微球直径来调控 AgMRs 的嵌套数量。图 4(c)表明,采用直径为 21  $\mu\text{m}$  的微球制备的三级嵌套 AgMRs 结构的拉曼增强性能优于其他直径微球制备的 AgMRs 结构,证明了 AgMRs 嵌套结构的增多有助于 SERS 衬底性能的提升。因此,在 98  $\mu\text{W}$  激光辐照功率下辐照 21  $\mu\text{m}$  微球 80 s 所制备的多级 AgNPs/AgMRs/MS 复合结构具有最佳的拉曼增强效果,其对 MB 水溶液的检出限可达  $10^{-14}$  mol/L,如图 4(d)所示。拉曼增强因子( $\zeta_{\text{EFRI}}$ )<sup>[44]</sup>的计算公式为

$$\zeta_{\text{EFRI}} = \frac{I_{\text{SERS}}}{I_0} \times \frac{C_0}{C_{\text{SERS}}}, \quad (1)$$

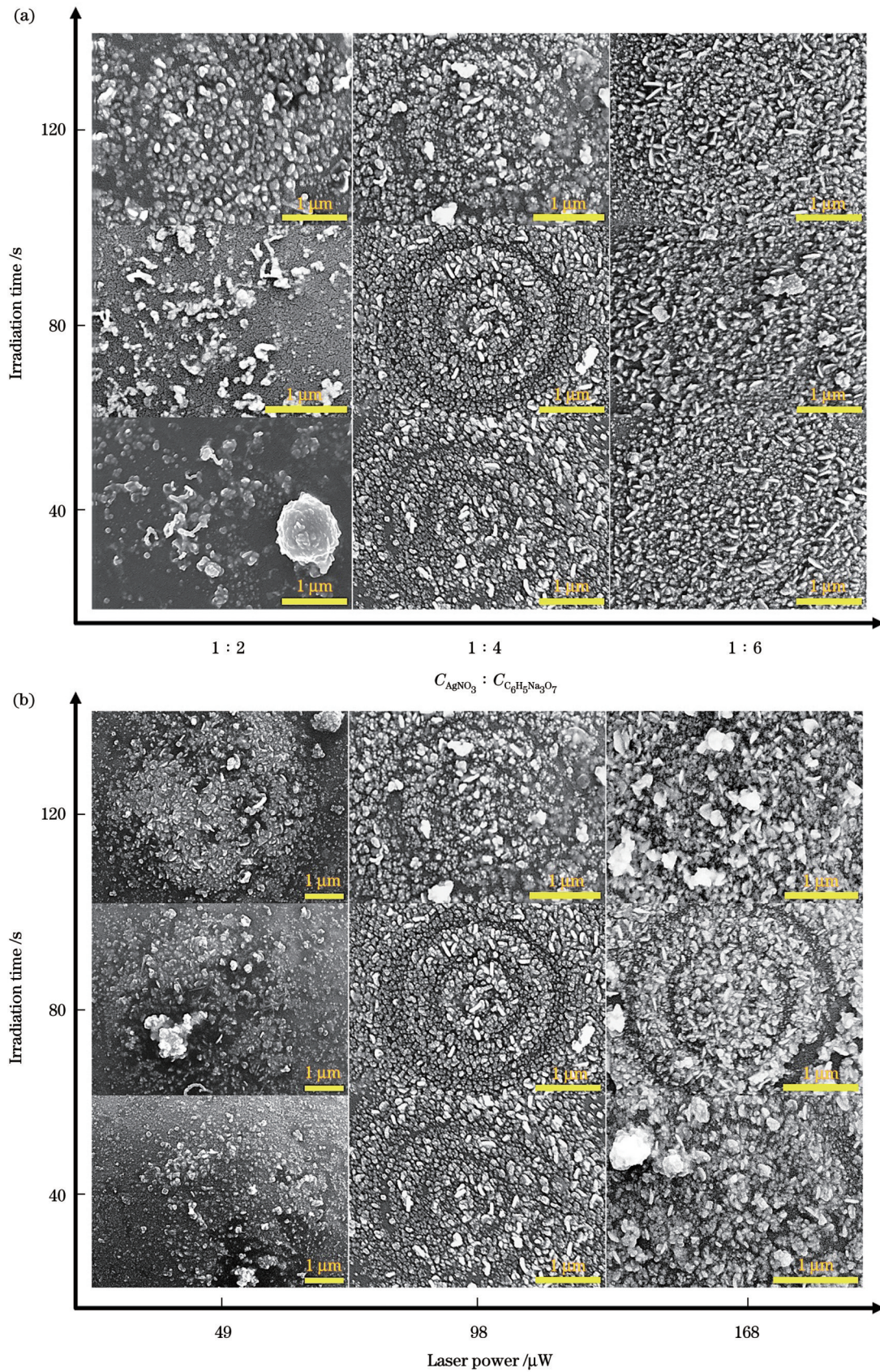


图 3 在不同光化学还原参数下多级银微纳结构表面的 SEM 显微图。(a) 多级银微纳结构随  $C_{AgNO_3} : C_{C_6H_5Na_3O_7}$  和辐照时间的变化；(b) 多级银微纳结构随激光辐照功率和辐照时间的变化

Fig. 3 SEM micrographs of hierarchical silver micro-nanostructure surfaces under different photochemical parameters. (a) Evolution of hierarchical silver micro-nanostructure with  $C_{AgNO_3} : C_{C_6H_5Na_3O_7}$  and irradiation time; (b) evolution of hierarchical silver nanostructure with laser irradiation power and irradiation time

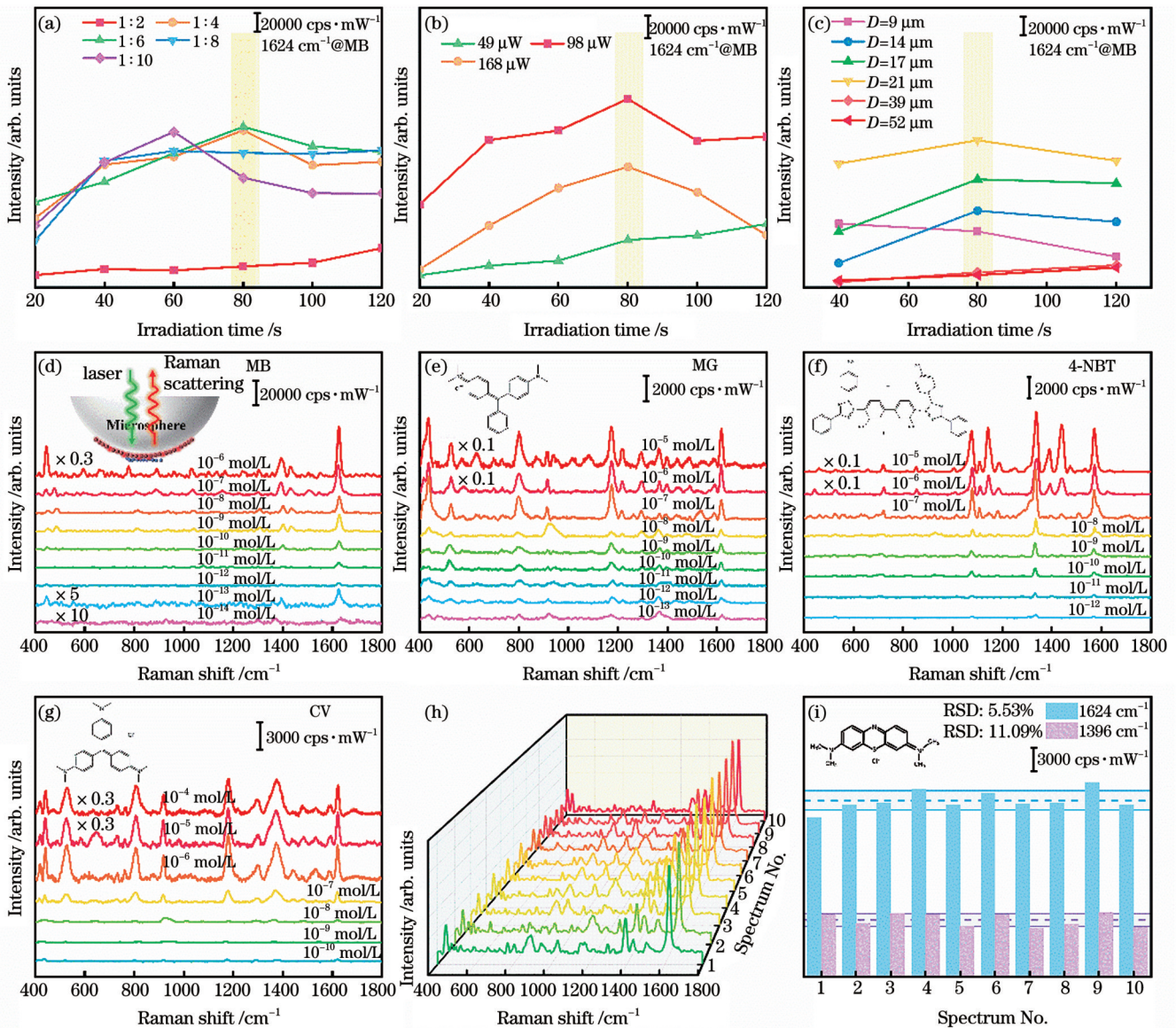


图 4 多级 AgNPs/AgMRs/MS 复合结构的 SERS 性能。(a)~(c) 激光化学还原参数  $C_{AgNO_3}:C_{C_6H_3Na_3O_7}$ 、辐照功率、微球直径对 MB 在  $1624\text{ cm}^{-1}$  处拉曼峰强度的调控规律；(d)~(g) MB 分子、MG 分子、4-NBT、CV 分子在多级 AgNPs/AgMRs/MS 复合结构 SERS 衬底上的拉曼检出限；(h) 多级 AgNPs/AgMRs/MS 复合结构的重复性测试；(i) MB 分子在  $1396\text{ cm}^{-1}$  和  $1624\text{ cm}^{-1}$  处的拉曼特征峰强度分布直方图

Fig. 4 SERS performance of hierarchical AgNPs/AgMRs/MS hybrid structures. (a)–(c) Regulation of the photochemical parameters  $C_{AgNO_3}:C_{C_6H_3Na_3O_7}$ , irradiation power, and microsphere diameter on Raman intensity of MB at  $1624\text{ cm}^{-1}$ ; (d)–(g) Raman detection limit of MB, MG, 4-NBT, and CV on hierarchical AgNPs/AgMRs/MS hybrid structures SERS substrate; (h) repeatability of hierarchical AgNPs/AgMRs/MS hybrid structures; (i) histogram of intensity distribution of Raman characteristic peaks at  $1396\text{ cm}^{-1}$  and  $1624\text{ cm}^{-1}$  for MB molecules

式中： $I_{SERS}$  和  $I_0$  分别为使用 SERS 衬底和未使用 SERS 衬底时检测到的拉曼强度； $C_{SERS}$  和  $C_0$  分别为使用 SERS 衬底和未使用 SERS 衬底时的溶液浓度。所获得的 AgNPs/AgMRs/MS 复合结构的最大拉曼增强因子为  $9.50 \times 10^9$ 。为进一步验证 AgNPs/AgMRs/MS 复合结构 SERS 衬底的普适性，检测了其对不同染料分子的拉曼检出限，如图 4(e)~(g) 所示。结果显示，AgNPs/AgMRs/MS 复合结构对孔雀石绿(MG)、4-硝基苯硫酚(4-NBT)、结晶紫(CV)的检出限分别为  $10^{-13}$ 、 $10^{-12}$ 、 $10^{-10}$  mol/L，展示出了其优异的拉曼检出

性能。此外，该 SERS 衬底还展现出了较好的重复性，如图 4(h)~(i) 所示，10 组 MB 分子在  $1396\text{ cm}^{-1}$  和  $1624\text{ cm}^{-1}$  处拉曼特征峰强度的相对标准偏差(RSD)分别为 11.09% 和 5.53%。

### 3.4 多级 AgNPs/AgMRs/MS 复合结构的拉曼增强机制

为了揭示多级 AgNPs/AgMRs/MS 复合结构的拉曼增强机制，分别在 Si、PDMS、MS、PDMS/MS、AgNPs、AgNPs/MS 等结构上进行了 MB 分子检出限测试。图 5(a) 为硅片上的 MB 分子检出限 ( $10^{-4}$  mol/L)。

覆盖 PDMS 后,由于激发光能量损耗,检出能力降低为  $10^{-3}$  mol/L,如图 5(b)所示。图 5(c)是使用微球时 MB 分子的检出限 ( $10^{-5}$  mol/L),即微球增强拉曼光谱 (MERS) 的增强因子  $\zeta_{\text{MERS}}$  为 5.74 (相较于 Si 衬底)。图 5(d)是微球嵌入 PDMS 后的检出限 ( $10^{-4}$  mol/L),相较于 PDMS 衬底,其增强因子为 6.19。上述实验结果表明介质微球具有一个数量级的拉曼增强能力。通过非相干光辐照化学还原制

备得到了 AgNPs 及 AgNPs/MS 结构,如图 5(e)所示,AgNPs 衬底的检出限为  $10^{-12}$  mol/L,增强因子  $\zeta_{\text{SERS}}$  为  $1.22 \times 10^7$  (相较于 Si 衬底),增强能力与 AgNPs 胶体一致<sup>[45-47]</sup>。当微球耦合 AgNPs 形成 AgNPs/MS 结构时,检出限下降一个数量级达到  $10^{-13}$  mol/L,如图 5(f)所示。进一步引入 AgMRs 结构后发现多级银微纳结构可使检出限进一步下降至  $10^{-14}$  mol/L,如图 4(d)所示。

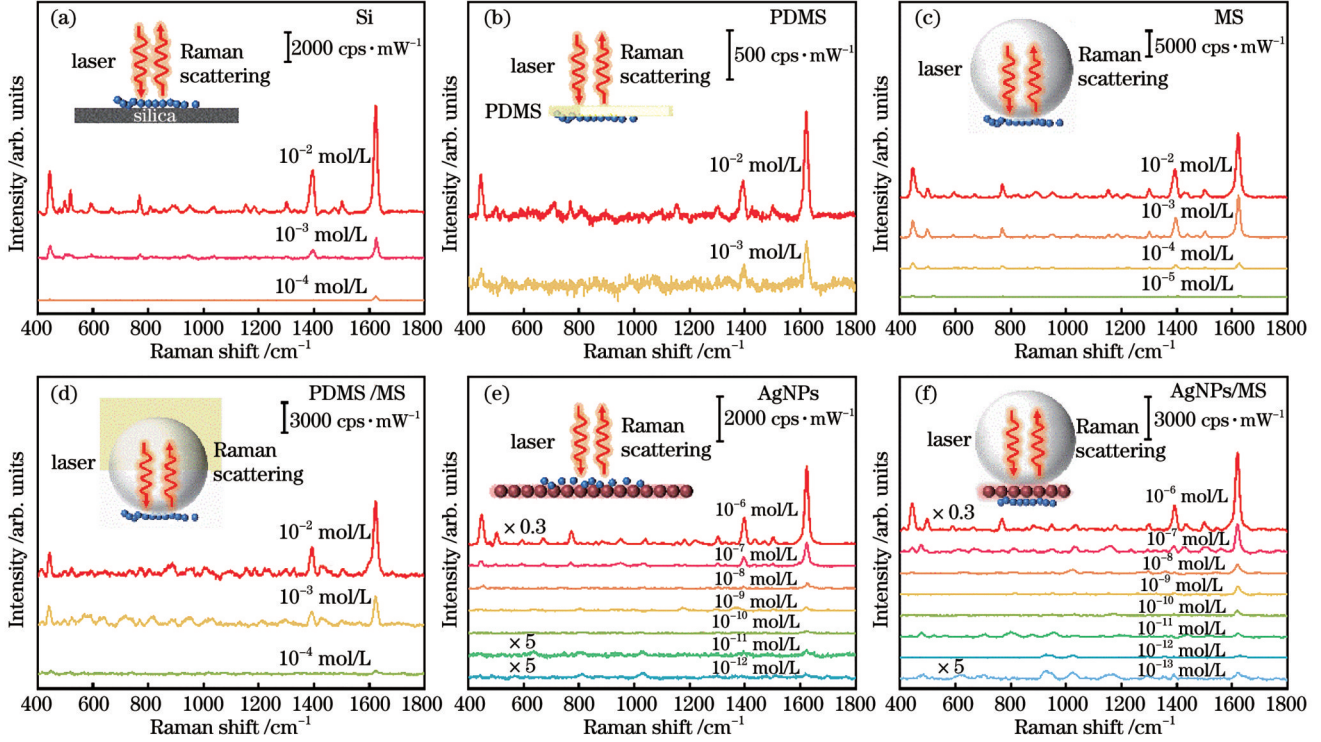


图 5 不同衬底上 MB 分子的拉曼检出限。(a) Si 衬底;(b) PDMS 衬底;(c) MS 衬底;(d) PDMS/MS 衬底;(e) AgNPs 衬底;(f) AgNPs/MS 衬底  
Fig. 5 Raman detection limit of MB molecules on different substrates. (a) Si substrate; (b) PDMS substrate; (c) MS substrate; (d) PDMS/MS substrate; (e) AgNPs substrate; (f) AgNPs/MS substrate

为了验证 AgMRs 在拉曼增强中的贡献,采用数值模拟研究了介质微球的聚焦效应、定向天线效应以及其与 AgMRs 局域表面等离子激元之间的耦合效应。介质微球的聚焦效应会提高激发光在微球底部的局域功率密度。图 6(a)~(b)展示了在 633 nm 激发波长下 AgNPs/AgMRs/MS 结构的光场强度分布以及底部聚焦电场强度分布曲线。可以看出,介质微球聚焦使激发光被局域在 AgMRs 结构缝隙中,电场强度显著提高,有利于提高拉曼散射的激发强度。接着,利用 AgNPs/AgMRs/MS 结构底部的总电场强度积分来评价远场激发光到近场的耦合效率,其中 AgMRs/MS 的增强因子  $\zeta_{\text{F}}$  可以通过式(2)进行估算<sup>[48]</sup>。

$$\zeta_{\text{F}} = \frac{2\pi \int_0^{r_p} |\mathbf{E}(r)|^2 r dr}{\pi r_p^2 |\mathbf{E}_0|^2}, \quad (2)$$

式中:  $\mathbf{E}_0$  和  $\mathbf{E}(r)$  分别为入射激光被介质微球聚焦之前

和之后的电场强度;  $r_p$  为微球半径。计算可得  $\zeta_{\text{F}} = 53.86$ , 这表明介质微球聚焦提高了 AgMRs 间局域表面等离子激元的电场强度,实现了对拉曼激发光的高效利用。此外,光学定向天线效应是介质微球对散射光场进行调控的主要手段<sup>[43]</sup>。图 6(c)展示了 MS 及 AgMRs/MS 结构定向天线的电场强度分布,可以看出 MS 和 AgMRs/MS 结构均显著增强了定向发射强度。图 6(d)所示的远场发射极坐标图表明散射光被局域在发散角为  $-6.52^\circ \sim +6.52^\circ$  的范围内,有效提高了光谱采集镜头对远场散射光的收集能力。通过式(3)可以计算得到定向天线效应对拉曼增强的贡献  $\zeta_{\text{DA}}$ <sup>[49]</sup>。

$$\zeta_{\text{DA}} = \frac{\int_0^{\arcsin(NA)} |\mathbf{E}'(\theta)|^2 \sin \theta d\theta}{\int_0^{\arcsin(NA)} |\mathbf{E}'_0(\theta)|^2 \sin \theta d\theta}, \quad (3)$$

式中:  $\mathbf{E}'_0(\theta)$  与  $\mathbf{E}'(\theta)$  分别是无 SERS 结构及 AgMRs/MS 结构的远场电场强度随角度的分布; NA 为显微物



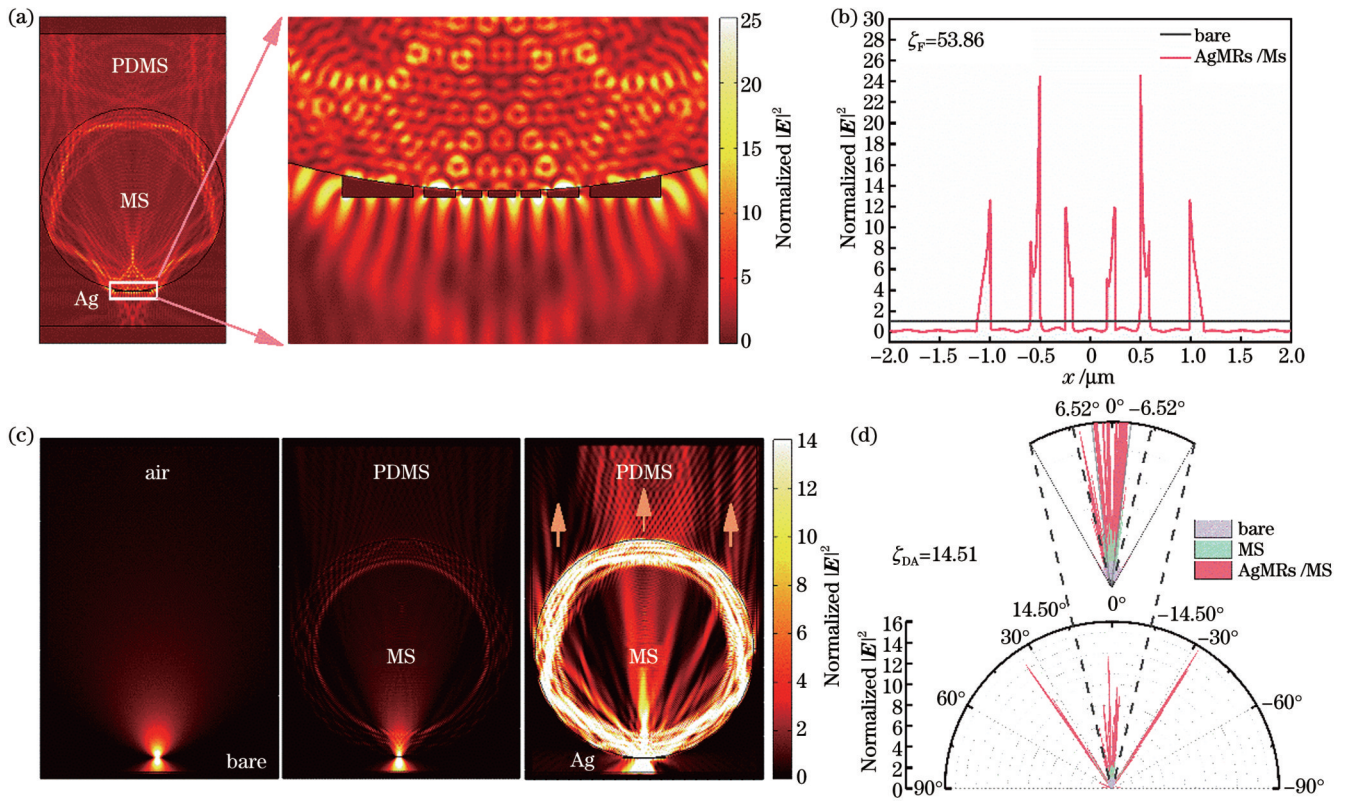


图 6 AgMRs/MS 结构聚焦效应及定向天线效应的数值模拟。(a) AgMRs/MS 结构的光场强度分布图; (b) AgMRs/MS 结构的聚焦光场强度分布曲线; (c) 自由空间、MS 及 AgMRs/MS 结构定向天线效应的光场强度分布图; (d) 自由空间、MS 及 AgMRs/MS 结构定向天线效应的远场发射极坐标图

Fig. 6 Numerical simulation of focusing effect and directional antenna effect of AgMRs/MS structure. (a) Optical field intensity distribution of the AgMRs/MS structure; (b) focused optical field intensity distribution curve of the AgMRs/MS structure; (c) optical field intensity distributions of directional antenna effect via the free space, MS and AgMRs/MS structures; (d) far-field emission polar plot of directional antenna effect via the free space, MS and AgMRs/MS structure

镜的数值孔径。计算可得 AgMRs/MS 结构的  $\zeta_{DA}=14.51$ 。为进一步阐释 AgMRs 结构对拉曼增强的贡献,对 MS 及 AgMRs/MS 的定向天线效应进行比较。将式(3)中的  $E'_0(\theta)$  改为 MS 的远场电场强度随角度的分布,计算得到  $\zeta_{DA-AgMRs}=6.61$ 。这表明 AgMRs 增强了远场散射定向发射能力,提供了除微球散射增强之外的额外增强。因此,AgNPs/AgMRs/MS 结构中 AgMRs 和 MS 所产生的总增强因子  $\zeta_F \times \zeta_{DA}=781.51$ 。进一步考虑到 AgNPs 中“热点”局域表面等离子体增强 ( $\zeta_{SERS}=1.22 \times 10^7$ ),则多级 AgNPs/AgMRs/MS 复合结构的增强因子  $\zeta$  为

$$\zeta = \zeta_{SERS} \times \zeta_F \times \zeta_{DA} = 9.53 \times 10^9. \quad (4)$$

这与实验结果相吻合,从而验证了多级 AgNPs/AgMRs/MS 复合结构的拉曼增强来源于微球聚焦、多级银微纳结构局域表面等离子体共振、复合结构定向发射这三重增强效应。

## 4 结 论

利用介质微球聚焦光场调控,在微球底部实现了快速激光化学还原多级银微纳结构的制备,并将该微纳结构应用于 SERS 痕量检测。研究表明,前驱液浓

度比、介质微球直径、激光功率、辐照时间均会对多级银微纳结构的形貌产生显著影响。采用直径为  $21 \mu\text{m}$  的钛酸钡微球,在前驱液浓度比  $C_{AgNO_3}:C_{C_6H_2Na_3O_7}=1:4$ 、 $532 \text{ nm}$  连续激光辐照功率为  $98 \mu\text{W}$ 、辐照时间为  $80 \text{ s}$  的条件下,可以获得具有最佳拉曼增强效果的多级 AgNPs/AgMRs/MS 复合结构。通过进一步的实验及数值模拟分析,揭示了多级 AgNPs/AgMRs/MS 复合结构的拉曼增强通道,即介质微球聚焦、多级银微纳结构局域表面等离子体共振以及复合结构定向发射增强。基于优化激光化学还原参数制备的多级 AgNPs/AgMRs/MS 复合结构,实现了增强因子为  $9.50 \times 10^9$ 、检出限为  $10^{-14} \text{ mol/L}$  的 SERS 衬底的快速制备。所提通过介质微球光场调控制备多级金属微纳结构的技术为低成本、高效率、结构多样的高灵敏介质-金属复合 SERS 衬底的制造提供了新思路。

## 参 考 文 献

- [1] Panneerselvam R, Liu G K, Wang Y H, et al. Surface-enhanced Raman spectroscopy: bottlenecks and future directions[J]. Chemical Communications, 2018, 54(1): 10-25.
- [2] Balčytis A, Nishijima Y, Krishnamoorthy S, et al. From fundamental toward applied SERS: shared principles and divergent

- approaches[J]. *Advanced Optical Materials*, 2018, 6(16): 1800292.
- [3] Tong Q, Wang W J, Fan Y N, et al. Recent progressive preparations and applications of silver-based SERS substrates[J]. *TrAC Trends in Analytical Chemistry*, 2018, 106: 246-258.
- [4] Zhang X G, Dai Z G, Si S Y, et al. Ultrasensitive SERS substrate integrated with uniform subnanometer scale "hot spots" created by a graphene spacer for the detection of mercury ions[J]. *Small*, 2017, 13(9): 1603347.
- [5] Li Z Y. Mesoscopic and microscopic strategies for engineering plasmon-enhanced Raman scattering[J]. *Advanced Optical Materials*, 2018, 6(16): 1701097.
- [6] 赖春红, 赖林, 张芝峻, 等. 基于金纳米颗粒-半胱胺 SERS 基底的水中硝酸根检测[J]. *中国激光*, 2022, 49(11): 1111002.
- Lai C H, Lai L, Zhang Z J, et al. Nitrate detection in water based on AuNPs-cysteamine SERS substrate[J]. *Chinese Journal of Lasers*, 2022, 49(11): 1111002.
- [7] Yu H D, Regulacio M D, Ye E Y, et al. Chemical routes to top-down nanofabrication[J]. *Chemical Society Reviews*, 2013, 42(14): 6006-6018.
- [8] Yu J, Wu J G, Yang H, et al. Extremely sensitive SERS sensors based on a femtosecond laser-fabricated superhydrophobic /-philic microporous platform[J]. *ACS Applied Materials & Interfaces*, 2022, 14(38): 43877-43885.
- [9] Wang A D, Jiang L, Li X W, et al. Low-adhesive superhydrophobic surface-enhanced Raman spectroscopy substrate fabricated by femtosecond laser ablation for ultratrace molecular detection[J]. *Journal of Materials Chemistry B*, 2017, 5(4): 777-784.
- [10] Bi K X, Chen Y Q, Wan Q, et al. Direct electron-beam patterning of transferrable plasmonic gold nanoparticles using a HAuCl<sub>4</sub>/PVP composite resist[J]. *Nanoscale*, 2019, 11(3): 1245-1252.
- [11] Li J F, Huang Y F, Ding Y, et al. Shell-isolated nanoparticle-enhanced Raman spectroscopy[J]. *Nature*, 2010, 464(7287): 392-395.
- [12] Sakamoto M, Fujituka M, Majima T. Light as a construction tool of metal nanoparticles: synthesis and mechanism[J]. *Journal of Photochemistry and Photobiology C: Photochemistry Reviews*, 2009, 10(1): 33-56.
- [13] 程自强, 石海泉, 余萍, 等. 银纳米颗粒阵列的表面增强拉曼散射效应研究[J]. *物理学报*, 2018, 67(19): 197302.
- Cheng Z Q, Shi H Q, Yu P, et al. Surface-enhanced Raman scattering effect of silver nanoparticles array[J]. *Acta Physica Sinica*, 2018, 67(19): 197302.
- [14] Kumar K V A, John J, Sooraj T R, et al. Surface plasmon response of silver nanoparticles doped silica synthesised via sol-gel route[J]. *Applied Surface Science*, 2019, 472: 40-45.
- [15] 白石, 周伟平, 马颖, 等. 紫外-可见光还原控制银纳米周期结构与形貌及其在表面增强拉曼散射中的应用[J]. *中国激光*, 2015, 42(3): 0303013.
- Bai S, Zhou W P, Ma Y, et al. Ag periodic nanostructures and morphology controlled by ultraviolet-visual photoreduction for surface-enhanced Raman scattering[J]. *Chinese Journal of Lasers*, 2015, 42(3): 0303013.
- [16] Ye S, Song J, Tian Y L, et al. Photochemically grown silver nanodecahedra with precise tuning of plasmonic resonance[J]. *Nanoscale*, 2015, 7(29): 12706-12712.
- [17] Stampelcoskie K G, Sciajno J C. Light emitting diode irradiation can control the morphology and optical properties of silver nanoparticles[J]. *Journal of the American Chemical Society*, 2010, 132(6): 1825-1827.
- [18] Wang T J, Barveen N R, Liu Z Y, et al. Transparent, flexible plasmonic AgNP/PMMA substrates using chemically patterned ferroelectric crystals for detecting pesticides on curved surfaces[J]. *ACS Applied Materials & Interfaces*, 2021, 13(29): 34910-34922.
- [19] Barveen N R, Wang T J, Chang Y H. Photochemical synthesis of Au nanostars on PMMA films by ethanol action as flexible SERS substrates for *in situ* detection of antibiotics on curved surfaces[J]. *Chemical Engineering Journal*, 2022, 431: 134240.
- [20] Yang L K, Yang J R, Li Y Y, et al. Controlling the morphologies of silver aggregates by laser-induced synthesis for optimal SERS detection[J]. *Nanomaterials*, 2019, 9(11): 1529.
- [21] Yoshikawa H, Hironou A, Shen Z J, et al. Versatile micropatterning of plasmonic nanostructures by visible light induced electroless silver plating on gold nanoseeds[J]. *ACS Applied Materials & Interfaces*, 2016, 8(36): 23932-23940.
- [22] Zheng Z K, Tachikawa T, Majima T. Single-particle study of Pt-modified Au nanorods for plasmon-enhanced hydrogen generation in visible to near-infrared region[J]. *Journal of the American Chemical Society*, 2014, 136(19): 6870-6873.
- [23] Lei Y T, Li D W, Zhang T C, et al. One-step selective formation of silver nanoparticles on atomic layered MoS<sub>2</sub> by laser-induced defect engineering and photoreduction[J]. *Journal of Materials Chemistry C*, 2017, 5(34): 8883-8892.
- [24] Linic S, Aslam U, Boerigter C, et al. Photochemical transformations on plasmonic metal nanoparticles[J]. *Nature Materials*, 2015, 14(6): 567-576.
- [25] MacKenzie M, Chi H N, Varma M, et al. Femtosecond laser fabrication of silver nanostructures on glass for surface enhanced Raman spectroscopy[J]. *Scientific Reports*, 2019, 9: 17058.
- [26] Ma Z C, Zhang Y L, Han B, et al. Femtosecond-laser direct writing of metallic micro/nanostructures: from fabrication strategies to future applications[J]. *Small Methods*, 2018, 2(7): 1700413.
- [27] Li C, Hu J, Jiang L, et al. Shaped femtosecond laser induced photoreduction for highly controllable Au nanoparticles based on localized field enhancement and their SERS applications[J]. *Nanophotonics*, 2020, 9(3): 691-702.
- [28] Liu L P, Yang D, Wan W P, et al. Fast fabrication of silver helical metamaterial with single-exposure femtosecond laser photoreduction[J]. *Nanophotonics*, 2019, 8(6): 1087-1093.
- [29] Yan W J, Yang L K, Chen J N, et al. *In situ* two-step photoreduced SERS materials for on-chip single-molecule spectroscopy with high reproducibility[J]. *Advanced Materials*, 2017, 29(36): 1702893.
- [30] 刘思垣, 张静宇. 基于空间光调制器的超快激光加工原理及应用[J]. *激光与光电子学进展*, 2020, 57(11): 111431.
- Liu S Y, Zhang J Y. Principles and applications of ultrafast laser processing based on spatial light modulators[J]. *Laser & Optoelectronics Progress*, 2020, 57(11): 111431.
- [31] Balena A, Bianco M, Pisanello F, et al. Recent advances on high-speed and holographic two-photon direct laser writing[J]. *Advanced Functional Materials*, 2023, 33(39): 2211773.
- [32] Chen Z G, Taflove A, Backman V. Photonic nanojet enhancement of backscattering of light by nanoparticles: a potential novel visible-light ultramicroscopy technique[J]. *Optics Express*, 2004, 12(7): 1214-1220.
- [33] Oraevsky A N. Whispering-gallery waves[J]. *Quantum Electronics*, 2002, 32(5): 377-400.
- [34] Devilez A, Stout B, Bonod N. Compact metallo-dielectric optical antenna for ultra directional and enhanced radiative emission[J]. *ACS Nano*, 2010, 4(6): 3390-3396.
- [35] Guo W, Wang Z B, Li L, et al. Near-field laser parallel nanofabrication of arbitrary-shaped patterns[J]. *Applied Physics Letters*, 2007, 90(24): 243101.
- [36] Lin Z Y, Liu K, Cao T, et al. Microsphere femtosecond laser sub-50 nm structuring in far field via non-linear absorption[J]. *Opto-Electronic Advances*, 2023, 6(6): 230029.
- [37] Yi K J, Wang H, Lu Y F, et al. Enhanced Raman scattering by self-assembled silica spherical microparticles[J]. *Journal of Applied Physics*, 2007, 101(6): 063528.
- [38] Yan Y Z, Xing C, Jia Y H, et al. Self-assembled dielectric microsphere array enhanced Raman scattering for large-area and

- ultra-long working distance confocal detection[J]. *Optics Express*, 2015, 23(20): 25854-25865.
- [39] Xing C, Yan Y Z, Feng C, et al. Flexible microsphere-embedded film for microsphere-enhanced Raman spectroscopy[J]. *ACS Applied Materials & Interfaces*, 2017, 9(38): 32896-32906.
- [40] Qian J S, Zhu Z B, Yuan J, et al. Selectively enhanced Raman/fluorescence spectra in photonic-plasmonic hybrid structures[J]. *Nanoscale Advances*, 2020, 2(10): 4682-4688.
- [41] Li X X, Lin X, Fang G Q, et al. Interfacial layer-by-layer self-assembly of PS nanospheres and Au@Ag nanorods for fabrication of broadband and sensitive SERS substrates[J]. *Journal of Colloid and Interface Science*, 2022, 620: 388-398.
- [42] Werner W S M, Glantschnig K, Ambrosch-Draxl C. Optical constants and inelastic electron-scattering data for 17 elemental metals[J]. *Journal of Physical and Chemical Reference Data*, 2009, 38(4): 1013-1092.
- [43] Mandal A, Dantham V R. Photonic nanojets generated by single microspheres of various sizes illuminated by resonant and non-resonant focused Gaussian beams of different waists[J]. *Journal of the Optical Society of America B*, 2020, 37(4): 977-986.
- [44] le Ru E C, Blackie E, Meyer M, et al. Surface enhanced Raman scattering enhancement factors: a comprehensive study[J]. *The Journal of Physical Chemistry C*, 2007, 111(37): 13794-13803.
- [45] Fan X Y, Zhang H, Zhao X R, et al. Three-dimensional SERS sensor based on the sandwiched G@AgNPs@G/PDMS film[J]. *Talanta*, 2021, 233: 122481.
- [46] Doan M Q, Anh N H, Quang N X, et al. Ultrasensitive detection of methylene blue using an electrochemically synthesized SERS sensor based on gold and silver nanoparticles: roles of composition and purity on sensing performance and reliability[J]. *Journal of Electronic Materials*, 2022, 51(1): 150-162.
- [47] Ansah I B, Lee S H, Mun C, et al. Nanoscale crack generation of Au/Ag nanopillars by *in situ* galvanic replacement for sensitive, label-free, and rapid SERS detection of toxic substances[J]. *Sensors and Actuators B: Chemical*, 2023, 379: 133172.
- [48] Wang M Y, Yan Y Z, Mi Y L, et al. Flexible microsphere-coupled surface-enhanced Raman spectroscopy (McSERS) by dielectric microsphere cavity array with random plasmonic nanoparticles[J]. *Journal of Raman Spectroscopy*, 2022, 53(7): 1238-1248.
- [49] Mi Y L, Yan Y Z, Wang M Y, et al. Cascaded microsphere-coupled surface-enhanced Raman spectroscopy (CMS-SERS) for ultrasensitive trace-detection[J]. *Nanophotonics*, 2022, 11(3): 559-570.

## Photochemical Synthesis Towards Hierarchical Silver Micro-Nanostructures via Dielectric Microspheres for Surface-Enhanced Raman Spectroscopy (Invited)

Chen Bingbing, Yan Yinzhou\*, Zhao Chen, Zhao Yan, Jiang Yijian

*Institute of Laser Engineering, Faculty of Materials and Manufacturing, Beijing University of Technology, Beijing 100124, China*

### Abstract

**Objective** Surface-enhanced Raman spectroscopy (SERS) harnesses metallic nanostructures combined with optical fields to create localized surface plasmon resonance (LSPR), yielding significant Raman scattering enhancement. However, “top-down” manufacturing methods for SERS substrates are often costly due to complex fabrication processes. Photochemical reduction synthesis, known for its high chemical purity and good process controllability, has gained attention but typically requires a high-power laser for rapid preparation. With advancements in high-power femtosecond-pulsed lasers, laser direct-writing has become viable for single-step SERS substrate fabrication. Nevertheless, the small focal laser spot limits efficiency in large-area fabrication of patterned micro-nanostructures. Dielectric microspheres, with their ability to focus incident lasers at their bottom beyond the diffraction limit, offer a solution for parallel nanomanufacturing. This study developed a one-step photochemical reduction technique for hierarchical silver micro-nanostructures using a dielectric microsphere array, demonstrating its ultra-sensitive Raman detection capability.

**Methods** A polydimethylsiloxane (PDMS) film was prepared by mixing PDMS with a curing agent and then spin-cured. Barium titanate microspheres, with high refractive indices (1.9), were pressed into a monolayer close-packed array on the PDMS film via mechanical grinding. An uncured PDMS film was placed onto this array, transferring and semi-embedding the microspheres into PDMS (PDMS/MS), followed by curing. The PDMS/MS film was then covered with a silver nitrate and trisodium citrate solution. A 532 nm line CW laser, with power ranging from 49–168  $\mu\text{W}$ , focused by PDMS/MS into the solution, induced the reduction reaction. Consequently,  $\text{Ag}^+$  was reduced under focused laser irradiation, forming a hierarchical silver micro-nanostructure (AgNPs/AgMRs) at the bottom of the microspheres. The surface morphology of the Ag micro-nanostructures was examined using SEM. The influence of microsphere diameter and photoreduction parameters on the morphology was both theoretically and experimentally investigated. Raman spectra of various analytes at different concentrations were acquired to optimize the hierarchical AgNP/AgMR/MS structure, with COMSOL simulations revealing the Raman enhancement mechanisms.

**Results and Discussions** The study explored how microsphere diameters affect the hierarchical Ag micro-nanostructure. With a

diameter increase to 21  $\mu\text{m}$ , AgMRs with three concentric circles were formed. Increasing the diameter further to 39  $\mu\text{m}$  resulted in the focused light energy at the microsphere bottom falling below the photochemical reduction threshold, leading to the formation of only a small amount of AgNPs (Fig. 2). Optimal photochemical reduction parameters were experimentally determined: a 1:4 molar concentration ratio of silver nitrate to trisodium citrate, a 98  $\mu\text{W}$  laser power, and an 80 s irradiation time produced clear AgMRs with high-density AgNPs at the microsphere bottom (Fig. 3). This configuration achieved a detection limit of  $10^{-14}$  mol/L for methylene blue solution and an enhancement factor ( $\zeta$ ) of up to  $9.50 \times 10^9$ . The SERS structure exhibited good reproducibility and compatibility for practical applications, as shown in Fig. 4. Furthermore, an enhancement factor of  $9.53 \times 10^9$  for the hierarchical AgNP/AgMR/MS structure was obtained through numerical simulation (Fig. 6), aligning well with experimental results. The Raman enhancement channels were attributed to electromagnetic enhancement from microsphere nanofocusing, localized surface plasmon resonances in AgNPs/AgMRs, and the directional antenna effect of the AgNPs/AgMRs/MS hybrid structure.

**Conclusions** This study proposes a new technique for fabricating hierarchical metal micro-nanostructures through optical field modulation of dielectric microspheres. Rapid photochemical reduction of the hierarchical Ag micro-nanostructure was achieved using the unique focusing properties of dielectric microspheres. The impact of precursor molar concentration ratio, microsphere diameter, laser power, and irradiation time on the morphology of the hierarchical Ag micro-nanostructures was thoroughly examined. An optimal Raman-enhancing hierarchical AgNP/AgMR/MS structure was fabricated using 21  $\mu\text{m}$  diameter barium titanate microspheres, a 1:4 silver nitrate to trisodium citrate molar concentration ratio, a 98  $\mu\text{W}$  laser power, and an 80 s irradiation time. Experiments and numerical simulations indicated that the Raman enhancement channels of the hierarchical AgNP/AgMR/MS structure stemmed from microsphere nanofocusing, localized surface plasmon resonance of the hierarchical Ag micro-nanostructure, and directional emission from the hybrid structure. The hierarchical AgNP/AgMR/MS hybrid structure demonstrated an enhancement factor of up to  $9.50 \times 10^9$  and a detection limit of  $10^{-14}$  mol/L for trace detection. This study provides a new strategy for creating ultra-sensitive dielectric/metal hybrid SERS substrates with low cost and high performance for practical applications.

**Key words** spectroscopy; surface-enhanced Raman spectroscopy; hierarchical silver micro-nanostructures; photochemical synthesis; dielectric microsphere